Sharpey-Schafer Prize Lecture

Structure and function of voltage-gated sodium channels at atomic resolution

William A. Catterall

Department of Pharmacology, University of Washington, Seattle, WA, USA

New Findings

- **What is the topic of this review?**
  The central goal of the research reviewed here is to understand the functional properties of voltage-gated sodium channels at the level of high-resolution structure of the channel protein.
- **What advances does it highlight?**
  The key functional properties of voltage-gated sodium channels, including voltage-dependent activation. Sodium conductance and selectivity, block by local anesthetics and related drugs, and both fast and slow inactivation, are now understood at the level of protein structure with high resolution. These emerging high-resolution structural models may lead to development of safer and more efficacious drugs for treatment of epilepsy, chronic pain, and cardiac arrhythmia through structure-based drug design.

Voltage-gated sodium channels initiate action potentials in nerve, muscle and other excitable cells. Early physiological studies described sodium selectivity, voltage-dependent activation and fast inactivation, and developed conceptual models for sodium channel function. This review article follows the topics of my 2013 Sharpey-Schafer Prize Lecture and gives an overview of research using a combination of biochemical, molecular biological, physiological and structural biological approaches that have elucidated the structure and function of sodium channels at the atomic level. Structural models for voltage-dependent activation, sodium selectivity and conductance, drug block and both fast and slow inactivation are discussed. A perspective for the future envisions new advances in understanding the structural basis for sodium channel function and the opportunity for structure-based discovery of novel therapeutics.

(Received 29 July 2013; accepted after revision 1 October 2013; first published online 4 October 2013)
Corresponding author W. A. Catterall: Department of Pharmacology, Box 357280, University of Washington, Seattle, WA 98195-7280, USA. Email: wcatt@u.washington.edu

Introduction

Sodium currents were first recorded as part of the analysis of the action potential of the squid giant axon using the voltage-clamp procedure (Hodgkin & Huxley, 1952*a*,*b*,*c*,*d*). That early work showed that electrical signals in nerves are initiated by voltage-dependent activation of sodium current that carries Na^+ inward and depolarizes the cell. The sodium current then inactivates within 1–2 ms, and electrical signalling is terminated by activation of the voltage-gated potassium current, which carries K^+ outward and re-establishes the original balance of electrical charges across the membrane. Much later work described a separate slow inactivation process for the sodium current in the squid giant axon, which developed in hundreds of milliseconds and reversed very slowly (Rudy, 1978). Studies of ion selectivity, saturation and block of sodium permeation led to a detailed model of the ion selectivity filter of the sodium channel and its function

The Sharpey-Schafer Prize Lecture was given on 24 July 2013 at IUPS 2013 in Birmingham, UK.

DOI: 10.1113/expphysiol.2013.071969

Experimental Physiology

in sodium selectivity (Hille, 1971, 1972, 1975*a*). The four-barrier, three-site model envisaged partial dehydration of Na^+ through interaction with a high-field-strength site containing a carboxyl side-chain at the extracellular end of the pore followed by rehydration in the lumen of the pore and escape into the intracellular milieu. This early work also established that local anaesthetics and related drugs that act on sodium channels bind to a receptor site in the pore of the channel, which can be accessed either through the open activation gate at the intracellular end of the pore or, for small hydrophobic drugs, through a membrane access pathway (Hille, 1977). Voltage sensitivity was proposed by Hodgkin and Huxley to depend on the movement of electrically charged particles, the gating charges, which were driven across the membrane by the change in voltage. Armstrong & Bezanilla (1973, 1974) used high-resolution electrophysiological recording methods to detect the transmembrane movement of the gating charges. Armstrong and colleagues also made key insights into the process of fast sodium channel inactivation, showing that it is mediated by protein components on the intracellular surface of the sodium channel that were hypothesized to fold into the pore and block it during inactivation (Armstrong *et al.* 1973; Armstrong & Bezanilla, 1977; Bezanilla & Armstrong, 1977). Together, the studies from many laboratories in the 1970s established enduring conceptual models of sodium channel function (reviewed by Armstrong, 1981; Hille, 2001), but there was no information on the structure of ion channel proteins at that time.

Discovery of the sodium channel protein

When I set up my laboratory at the University of Washington, the main new goal was to identify and purify the sodium channel molecule. Through the 1970s, work in several laboratories had demonstrated that neurotoxins act on multiple receptor sites to modify the ion conductance and voltage-dependent gating of sodium channels (reviewed by Catterall, 1980). In 1980, we identified the protein subunits of the sodium channel by photoaffinity labelling with scorpion toxin derivatives (Beneski & Catterall, 1980), revealing large α subunits of 260 kDa and smaller β subunits of 30–40 kDa (Fig. 1). After solubilization and purification, brain sodium channels were found to contain an α subunit with a non-covalently associated $\beta 1$ subunit and a disulfide-linked $\beta 2$ subunit (Fig. 1; Hartshorne & Catterall, 1981, 1984; Hartshorne *et al.* 1982), and this purified complex was sufficient to reconstitute voltage-gated sodium (Na_V) channel function with the correct pharmacology, single-channel conductance and voltage sensitivity after insertion into phospholipid vesicles and bilayers (Fig. 1; Talvenheimo *et al.* 1982; Tamkun *et al.* 1984; Hartshorne *et al.* 1985). These studies provided the first identification and functional reconstitution of a voltage-gated ion channel protein and established the principle that these ion channels are composed of primary pore-forming subunits in association with auxiliary subunits.

Primary structures of sodium channel subunits

Cloning and sequencing of cDNA encoding the α subunits of sodium channels defined their primary structures and showed that mRNA encoding the α subunit is sufficient for expression of functional sodium channels (Noda *et al.* 1984, 1986; Goldin *et al.* 1986). Sodium channel α subunits are composed of approximately 2000 amino acid residues organized in four homologous domains, each of which contains six transmembrane segments (Fig. 2). Later biochemical analyses and cDNA cloning showed that sodium channel β subunits are composed of an N-terminal extracellular immunoglobulin-like fold, a single transmembrane segment and a short intracellular segment (Fig. 2; Isom *et al.* 1992, 1995). These subunits are thought to form heterodimeric and heterotrimeric complexes composed of a single α subunit and one or two β subunits in excitable cell membranes. Coexpression of β subunits modulates the kinetics and voltage dependence of sodium channel activation and inactivation, and the extracellular immunoglobulin domains of β subunits serve as cell adhesion molecules that interact with

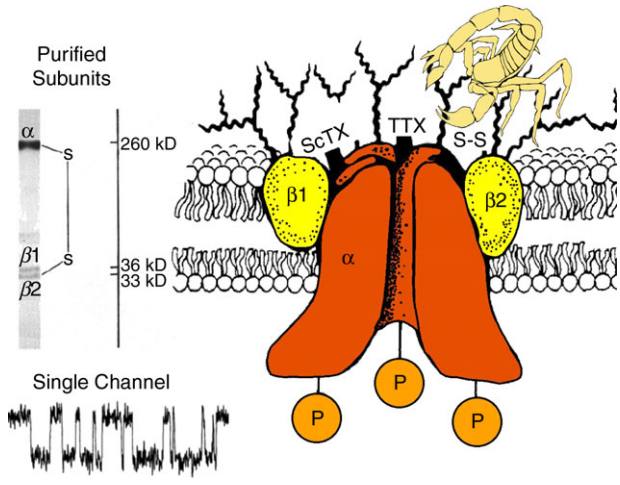

Figure 1. Subunit structure of voltage-gated sodium channels
Sodium dodecyl sulfate-polyacrylamide gel electrophoresis pattern illustrating the α and β subunits of the brain sodium channels. As illustrated, the α and $\beta 2$ subunits are linked by a disulfide bond. Tetrodotoxin (TTX) and scorpion toxins (ScTX)bind to the α subunits of sodium channels as indicated and were used as molecular tags to identify and purify the sodium channel protein (Beneski & Catterall, 1980; Hartshorne *et al.* 1982; Hartshorne & Catterall, 1984). Bottom left panel, single-channel currents conducted by a single purified sodium channel incorporated into a planar bilayer (Hartshorne *et al.* 1985).

extracellular matrix proteins and other cell adhesion molecules (Isom *et al.* 1992, 1995; Srinivasan *et al.* 1998; Malhotra *et al.* 2000; Ratcliffe *et al.* 2000, 2001; Kazarinova-Noyes *et al.* 2001; Brackenbury & Isom, 2011).

The voltage-gated ion channel protein superfamily

Analysis of the human genome revealed that there are 143 ion channel proteins whose pore-forming segments are related to sodium channels, and they are associated with at least 10 distinct families of auxiliary subunits (Yu & Catterall, 2004). The voltage-gated ion channels and their molecular relatives are one of the largest superfamilies of signalling proteins and one of the most prominent targets for drugs. Surprisingly, the sodium channel family is ancient in evolution. The bacterial sodium channel NaChBac and several prokaryotic relatives are composed of homotetramers of a single subunit whose structure resembles one of the domains of a vertebrate sodium or calcium channel (Ren *et al.* 2001; Koishi *et al.* 2004). It is likely that these bacterial sodium channels are the evolutionary ancestors of the larger, much more complex, four-domain sodium and calcium channels in eukaryotes (Yu & Catterall, 2004).

Sodium channel structure at atomic resolution

Sodium channel architecture has recently been revealed in three dimensions by determination of the crystal structure of the bacterial sodium channel Na_VAb at high resolution (2.7 Å; Fig. 3; Payandeh *et al.* 2011). This structure has revealed a wealth of new information about the structural basis for voltage-dependent activation, pore opening, sodium selectivity and conductance, the mechanism of block of the channel by therapeutically important drugs and the mechanism of inactivation. As viewed from the top, Na_VAb has a central pore surrounded by four pore-forming modules composed of S5 and S6 segments and

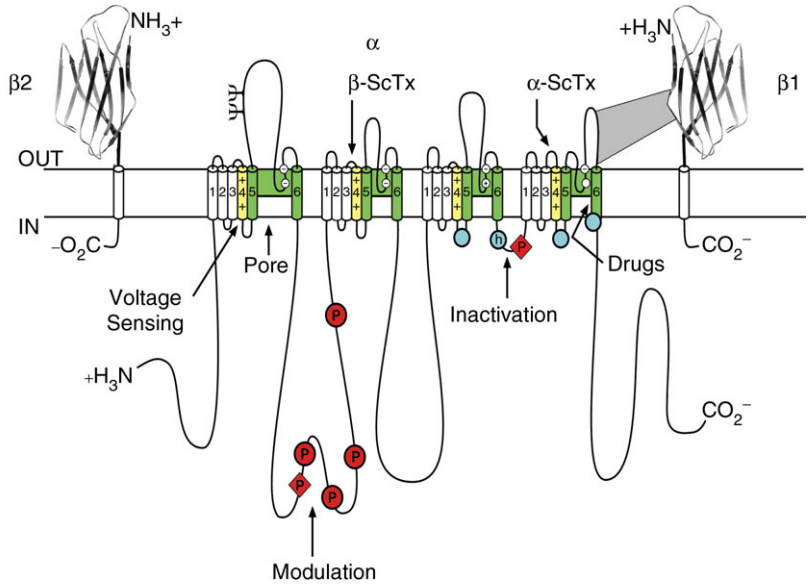

Figure 2. The primary structures of the subunits of the voltage-gated sodium channels
Cylinders represent α-helical segments. Bold lines represent the polypeptide chains of each subunit with length approximately proportional to the number of amino acid residues in the brain sodium channel subtypes. The extracellular domains of the β1 and β2 subunits are shown as immunoglobulin-like folds. Symbols: Ψ, sites of probable N-linked glycosylation; P in red circles, sites of demonstrated protein phosphorylation by protein kinase A (PKA; circles) and protein kinase C (PKC) (diamonds); green, pore-lining segments; white circles, the outer (EEEE) and inner (DEKA) rings of amino residues that form the ion selectivity filter and the tetrodotoxin binding site; yellow, S4 voltage sensors; h in blue circle, inactivation particle in the inactivation gate loop; and blue circles, sites implicated in forming the inactivation gate receptor (Catterall, 2000). Sites of binding of α- and β-scorpion toxins and a site of interaction between α and β1 subunits are also shown. Tetrodotoxin is a specific blocker of the pore of sodium channels (Hille, 1975*b*), whereas the α- and β-scorpion toxins block fast inactivation and enhance activation, respectively, and thereby generate persistent sodium current that causes depolarization block of nerve conduction (Catterall *et al.* 2007). Tetrodotoxin has been used as a tool to probe the pore of the sodium channel, whereas the scorpion toxins have been valuable as probes of voltage sensor function.

the intervening pore loop (Fig. 3*A*, blue tones). Four voltage-sensing modules composed of S1–S4 segments are symmetrically associated with the outer rim of the pore module (Fig. 3*A*, warm colours). The transmembrane architecture of Na_VAb shows that the adjacent subunits have swapped their functional domains such that each voltage-sensing module is most closely associated with the pore-forming module of its neighbour, similar to voltage-gated potassium (K_V) channels (Long *et al.* 2007). It is likely that this domain-swapped arrangement enforces concerted gating of the four subunits or domains of sodium and potassium channels. The architecture of the Na_VAb pore reveals a wide outer vestibule, a narrow ion selectivity filter, a large central cavity and an intracellular activation gate formed by the crossing of S6 segments, which is in the closed position in Na_VAb (Fig. 3*B*). The P helix supporting the ion selectivity filter is similar to the P helix in K_V channels, whereas the P2 helix is unique to Na_V channels and supports the outer vestibule. This general pore architecture reveals the structural basis for gated access of blocking ions and drugs to the lumen of the pore observed in classical studies of ion selectivity and pore block (Armstrong, 1971; Hille, 1975*a*, 1977). The tight closure of the pore illustrates why the pore must be opened to allow drug access to the receptor site(s) within it.

Voltage sensing and voltage-dependent activation

Voltage-dependent activation of sodium channels was first demonstrated by Hodgkin and Huxley, and they predicted that the steep voltage dependence of sodium channel activation would require movement of three 'electrically charged particles' across the cell membrane through the full extent of the transmembrane electric field (Hodgkin & Huxley, 1952*d*). The predicted transmembrane movement of these gating charges was detected as a small capacitative gating current in high-resolution voltage-clamp studies of the squid giant axon (Armstrong & Bezanilla, 1973, 1974; Keynes & Rojas, 1974), fulfilling a major tenet of the Hodgkin–Huxley model for channel function. The S4 transmembrane segments of sodium channels contain four to seven repeated motifs of a positively charged amino acid residue (usually arginine) followed by two hydrophobic residues. They were proposed to carry the gating charges of sodium channels in the 'sliding helix' or 'helical screw' model of voltage sensing (Catterall, 1986*a*,*b*; Guy & Seetharamulu, 1986; Yarov-Yarovoy *et al.* 2006). In this model, the S4 segment is proposed to be in a transmembrane position in both resting and activated states, the gating charges are stabilized by forming ion pairs with neighbouring negatively charged residues, and their outward movement is catalysed by exchange of these ion pair partners (Catterall, 1986*a*,*b*; Guy & Seetharamulu, 1986; Yarov-Yarovoy *et al.* 2006, 2011; Shafrir *et al.* 2008). Extensive studies of sodium channels now provide strong support for all of the elements of this model (reviewed by Catterall, 2010).

Mutation of the arginine residues in the S4 segment of sodium channels reduces the steepness of voltage-dependent gating, consistent with the idea that these residues serve as gating charges (Stühmer *et al.* 1989; Kontis *et al.* 1997). The transmembrane position of the S4 segment in sodium channels has been confirmed by mapping the receptor sites for scorpion toxins in detail and showing that these toxins bind to the outer end of the S3–S4 loop of the voltage sensors in both resting and activated states, thereby establishing that the S4 segment remains in a transmembrane position in both of these

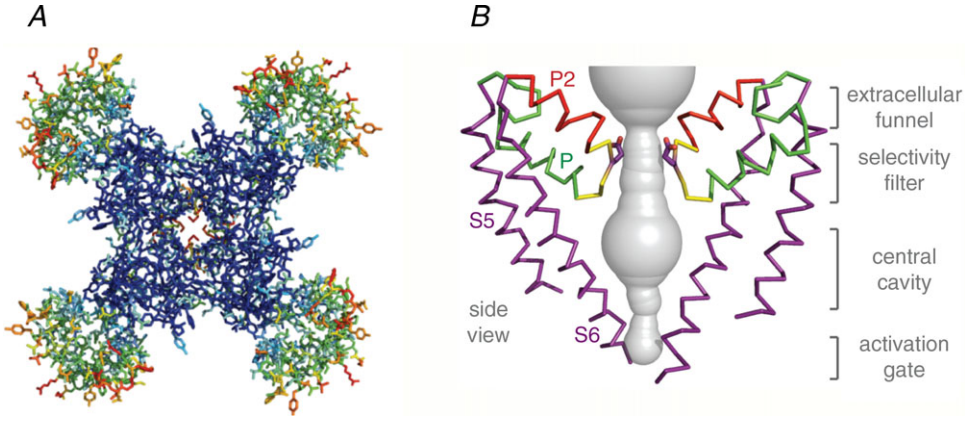

Figure 3. Structure of Na_VAb channel
A, top view of Na_VAb channels coloured according to crystallographic temperature factors of the main chain (blue < 50 Å^2 to red > 150 Å^2). *B*, architecture of the Na_VAb pore, with colours as follows: purple, Glu177 side-chains; and grey, pore volume. The S5 and S6 segments and the P loop from two lateral subunits are shown (Payandeh *et al.* 2011).

states (Catterall, 1979; Rogers *et al.* 1996; Cestèle *et al.* 1998, 2006; Wang *et al.* 2011; Zhang *et al.* 2011). Covalent labelling and voltage-clamp fluorescence studies show that the S4 segments of sodium channels move outward and rotate upon membrane depolarization and transport the gating charges from an inner water-accessible vestibule to an outer water-accessible vestibule (Yang & Horn, 1995; Yang *et al.* 1996; Chanda & Bezanilla, 2002). Molecular modelling of sodium channel voltage sensors with rigid scorpion toxins bound has yielded high-resolution models of the voltage sensor in its resting and activated states (Wang *et al.* 2011; Zhang *et al.* 2011), which also illustrate the outward movement of the S4 segment and exchange of ion pair partners in the transition from resting to activated states.

The X-ray crystal structures of the $K_V1.2$ and Na_VAb channels provide high-resolution models of activated voltage sensors (Fig. 4*A*; Long *et al.* 2005*a*; Payandeh *et al.* 2011). The four transmembrane helices are organized in two helical hairpins composed of the S1–S2 and the S3–S4 transmembrane segments. The four gating-charge-carrying Arg residues in the S4 segment (R1–R4 in Na_VAb; yellow in Fig. 4) are arrayed in a sequence across the membrane. Immediately below the centre of the four-helix bundle, a cluster of hydrophobic residues, including a highly conserved phenylalanine residue (Phe56 in Na_VAb), form the hydrophobic constriction site (HCS), which seals the voltage sensor to prevent transmembrane movement of water and ions (Fig. 4*A*, green). An analogous Phe residue is crucial for voltage sensor function in K_V channels (Tao *et al.* 2010). Gating charges R1–R3 are located on the extracellular side of the HCS, and their Arg side-chains interact with the negatively charged side-chains of the extracellular negative cluster (ENC; Fig. 4*A*, red). Gating charge R4 is located on the intracellular side of the HCS and interacts with the intracellular negative cluster (INC; Fig. 4*A*, red). Overall, the structure of the voltage sensor seems designed to catalyse movement of the S4 gating charges through the HCS, exchanging ion pair partners between the INC and ENC.

The voltage sensor in the Na_VAb structure has three of its gating charges on the extracellular side of the HCS (Fig. 4*A*; Payandeh *et al.* 2011). This conformation is nearly identical to the conformation of the voltage sensor in the structure of the $K_V1.2$ channel in its open state (Long *et al.* 2005*a*,*b*). Nevertheless, the activation gate of Na_VAb is tightly closed by interaction of the side-chains of Met221 (Fig. 3*B*). Therefore, it is likely that the Na_VAb structure has captured the pre-open state, which is an expected intermediate in the activation process in which all four voltage sensors have been activated by depolarization and the intracellular activation gate is still closed, but poised to open rapidly in a concerted conformational change of all four subunits.

Although the structure of the activated voltage sensor is now well known, understanding the mechanism of

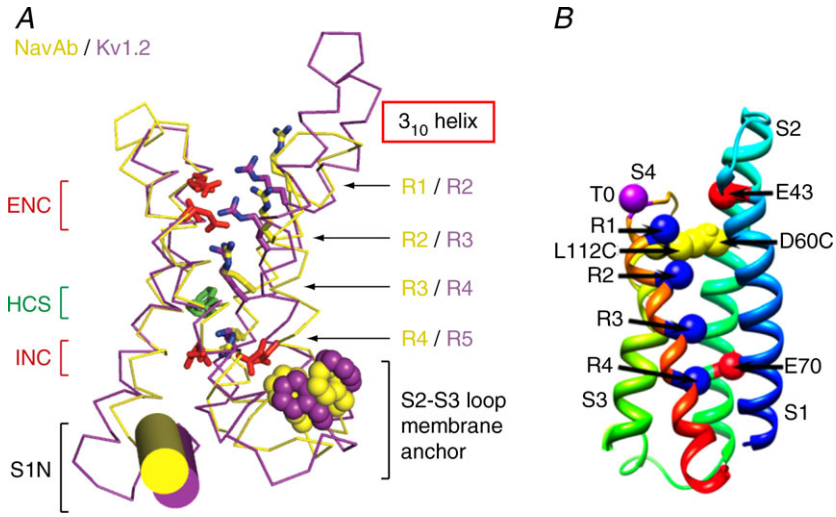

Figure 4. Structure of the voltage sensor
A, structure of the voltage sensor in an activated state. Side views of the structures of Na_VAb (yellow; Payandeh *et al.* 2011) and $K_V1.2$ (purple; Long *et al.* 2005*a*) are superimposed. Colours and abbreviations are as follows: red, extracellular negative cluster (ENC); green, hydrophobic constriction site, (HCS); and red, intracellular negative cluster (INC). *B*, model of the resting state of the NaChBac voltage sensor. Gating charges R1–R4 are shown as blue circles; T0, Thr in the position of the R0 gating charge in some K_V channels; L112C, Cys substituted for Leu adjacent to R1 in S4 segment forming a disulfide bond with Cys substituted for Asp60 (D60C) in S2 segment in the resting state as observed in disulfide locking experiments; E43, Glu 43 in S1 segment, a component of the extracellular negative cluster; and E70, Glu70 in S2 segment, a component of the intracellular negative cluster.

voltage-dependent gating requires knowledge of the structure of the voltage sensor in its resting state at high resolution. This structure has proved difficult to define by X-ray crystallography because the resting state is only present in cells at the resting membrane potential of approximately −80 mV, and there is no membrane potential in protein crystals. We have used molecular modelling methods to gain initial insight into the structures of resting and intermediate states of the voltage sensor. *Ab initio* molecular modelling using the ROSETTA algorithm provided a detailed structural model of the resting states of the voltage sensor and charted the sequence of conformational changes and gating charge interactions with negative charges and hydrophilic groups in the voltage sensor during activation (Fig. 4*B*; Yarov-Yarovoy *et al.* 2006, 2011). These structural models show that the S4 segment and its gating charges move through a narrow gating pore at the HCS that focuses the transmembrane electric field to a distance of approximately 5 Å normal to the membrane and allows the gating charges to move from an intracellular aqueous vestibule to an extracellular aqueous vestibule with a short transit through the channel protein, as proposed from structure–function studies (Starace & Bezanilla, 2004; Chanda *et al.* 2005). A structurally realistic gating movie based on these ROSETTA structural models captures the essence of the transmembrane movement of the gating charges (Supplemental Movie S1; Yarov-Yarovoy *et al.* 2011).

This mechanism of outward movement of the gating charges during the activation process has been confirmed by extensive disulfide-locking studies of the ion-pair interactions in sodium channels predicted from the sliding helix model of gating (Yarov-Yarovoy *et al.* 2006, 2011; DeCaen *et al.* 2008, 2009, 2011). For example, the R3 gating charge is predicted to be far from Asp60 in the ENC in the resting state (Fig. 4*B*), but to move into close proximity to Asp60 in the activated state (Supplemental Movie S1; Yarov-Yarovoy *et al.* 2011). This model predicts that Cys residues substituted at these two positions in the Cys-free background of NaChBac would not form a disulfide bond in the resting state but would rapidly form a disulfide bond in the activated state and cause persistent inactivation of the channel. Wild-type NaChBac channels or channels with single R3C or D60C substitutions conduct sodium current consistently during repetitive depolarizations (Fig. 5*A*). In contrast, the double Cys mutant R3C:D60C conducts a normal sodium current on its first depolarization but then inactivates and does not respond to depolarization again until the disulfide bond is reduced with β-mercaptoethanol (Fig. 5*A*). Tests with depolarizations of increasing duration in the millisecond time scale show that the rate of disulfide locking is nearly identical to the rate of pore opening (Fig. 5*B*), confirming that the disulfide bond is formed immediately upon voltage sensor activation.

In contrast to the R3:D60 ion pair, residues Val109 and Leu112 immediately preceding the R1 and R2 gating charges are predicted to be close to Asp60 in the resting state (Fig. 4*B*) but not in the activated state (Supplemental Movie S1; Yarov-Yarovoy *et al.* 2011). In this case, the sliding helix gating model predicts that these pairs of residues would form disulfide bonds in the resting state of the voltage sensor such that no sodium current would be observed upon initial stimulation of the channel, but sodium current would appear during repetitive depolarizations in the presence of β-mercaptoethanol to reduce the preformed disulfide bonds. Indeed, the D60C:V109C and D60C:L112C double mutants behave exactly as predicted (Yarov-Yarovoy *et al.* 2011), confirming the interactions between these two pairs of residues in the resting state. Together, these results indicate that gating charges R1 and R2 are in position to interact with the ENC in the resting state, whereas R3 is in position to interact with the ENC only in the activated state. This sequence of interactions of all residues in S4 with Asp60 can be predicted from the structure of the resting state of the voltage sensor (Fig. 4*B*). Evidently, amino acid residues at the extracellular end of the S4 segment are in position to interact with Asp60 in the ENC in the resting state, whereas amino acid residues at the intracellular end of S4 can interact only in the activated state.

Studies of the interactions of gating charges with Asp60 in the ENC near the extracellular end of the S2 segment and with Glu70 in the INC near the intracellular end of the S2 segment also demonstrated sequential exchange of ion-pair partners during activation of the voltage sensor (DeCaen *et al.* 2009). The innermost gating charge, R4, does not interact with either Glu70 or Asp60 in the resting state. However, upon depolarization, R4 is disulfide locked with Glu70 in the INC and Asp60 in the ENC on the millisecond time scale. It reacts with Glu70 more rapidly and at more negative membrane potentials than with Asp60, as expected from the more intracellular position of Glu70 in the S2 segment (DeCaen *et al.* 2009).

Similar results are observed for interactions of the R1–R4 gating charges with Glu43 in the S2 segment, the second conserved negatively charged residue in the ENC of NaChBac (Fig. 4*B*). The R1C disulfide locks with Glu43 in the resting state (Fig. 5*C*). Seventy per cent of R2C forms a disulfide bond with Glu43 in the resting state, and the remainder is induced to disulfide lock by repetitive pulses that generate the activated state (Fig. 5*D*). These results indicate that R2 can adopt two distinct conformations in the resting state, one with its side-chain near Glu43 and one in which its side-chain is on the intracellular side of Glu43. The R3 disulfide locks with Glu43 only in the activated state (Fig. 5*E*). However, R4 cannot be disulfide

locked with Glu43, suggesting that this interaction is beyond the range of outward movement of R4. These results demonstrate sequential interaction of the R1–R3 gating charges with Glu43 as the channel moves from the resting to the activated state.

In order to compare the voltage dependence of disulfide locking of different Cys double mutants, we also determined the extent of disulfide locking at a range of membrane potentials and normalized to the voltage dependence of pore opening to correct for intrinsic differences in voltage-dependent gating (DeCaen, PG 2010). When compared in this way, there is a close correlation of the voltage dependence of the pairwise interactions between amino acid residues in the S4 segment and interacting partners in the S1 and S2 segments, and the positions of these voltage dependence curves on the voltage axis follows the sequence of interactions expected in the sliding helix model of voltage sensor function. Together, these studies define the detailed mechanism of voltage-dependent activation of the voltage sensor of sodium channels through a series of resting and activated states involving an outward movement of the S4 segment of approximately 10 Å (Supplemental Movie S1; Yarov-Yarovoy *et al.* 2011). The sliding helix model is also consistent with metal ion and sulfhydryl crosslinking studies of *Shaker* potassium

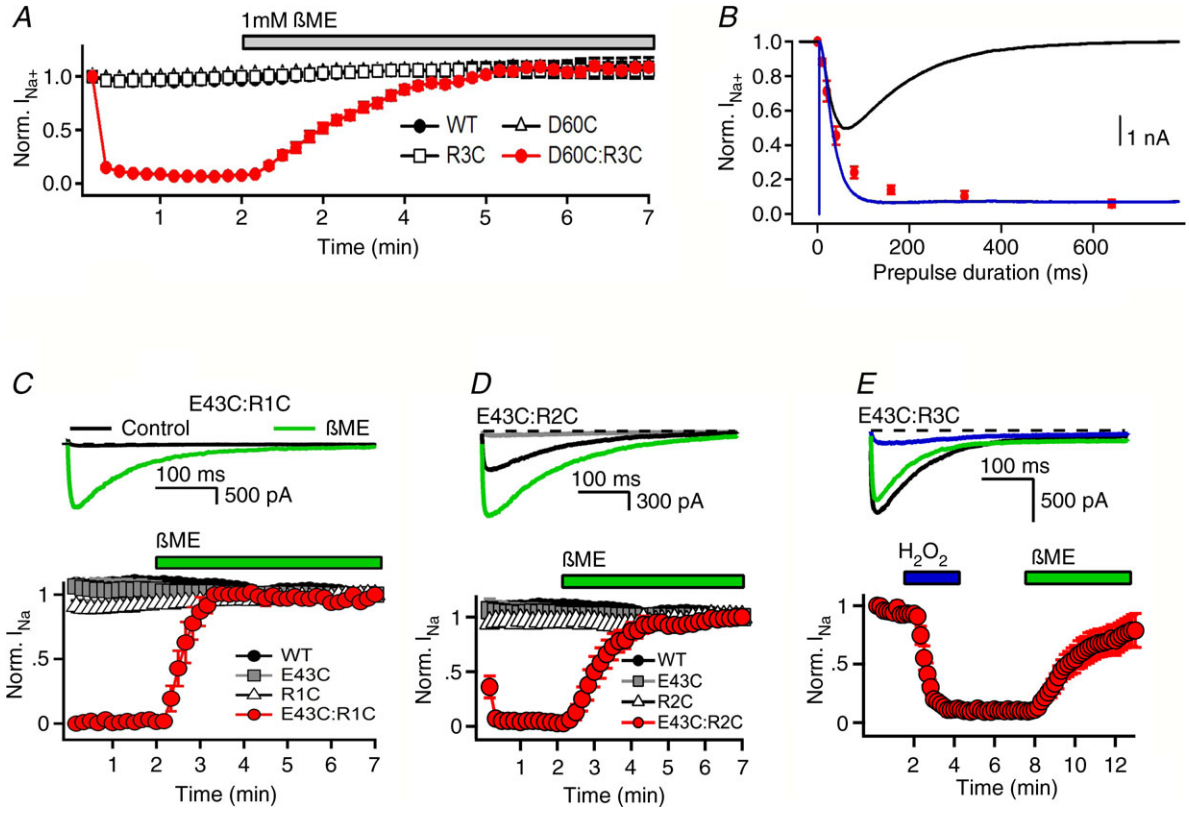

Figure 5. Disulfide locking the voltage sensor in resting and activated states
The NaChBac wild-type (WT), single Cys mutants D60C and R3C, and double Cys mutant D60C:R3C were expressed in tsA-201 cells and recorded using the whole-cell voltage-clamp mode. *A*, reversible disulfide locking. Mean normalized peak currents elicited by a 0.1 Hz train of 500 ms depolarizations to 0 mV from a holding potential of −140 mV in tsA cells transfected with D60C, R3C or D60C:R3C channels. After 2 min in control saline conditions, cells were exposed to 1 mM β-mercaptoethanol (βME; DeCaen *et al.* 2008). *B*, time course of voltage-sensor locking. The D60C:R3C channels were first unlocked by a 5 s prepulse to −160 mV. Cells were then depolarized for the indicated times to approximately $V_{1/2}$ + 20 mV (WT, −20 mV; D60C and R3C, 0 mV; and D60C:R3C, −30 mV), returned to −120 mV for 5 s and depolarized for a 100 ms test pulse to 0 mV. Peak test pulse current at 0 mV was normalized to the control pulse current in the absence of a prepulse and mean (±SEM) was plotted *versus* prepulse duration (red circles with error bars). Also shown are the sodium current recorded during a −30 mV prepulse (black continuous line) and the time course of activation in the absence of inactivation (blue trace) estimated by fitting an exponential to the current decay and adding the inactivated component back to the total current (DeCaen *et al.* 2008). *C*, disulfide locking of R1 and Glu43 in the resting state. *D*, disulfide locking of R2 and Glu43 in resting and activated states. *E*, disulfide locking of R3 and Glu43 in the activated state. Disulfide locking was induced by depolarization in the presence of 1 mM H_2O_2 (DeCaen *et al.* 2011).

channels (Campos *et al.* 2007; Broomand & Elinder, 2008; Lin *et al.* 2011), and a consensus of several groups using different structural modelling methods supports this voltage-sensing mechanism (Vargas *et al.* 2012).

Pore opening

In our crystal structure, Na_VAb has been captured in the pre-open state with all four voltage sensors activated, and the pore still closed but poised for rapid and concerted opening. In contrast, the $K_V1.2$ structure has nearly identical conformation of the voltage sensor but has an open pore (Long *et al.* 2005*a*). We have inferred the structural changes that cause pore opening by comparing the Na_VAb and $K_V1.2$ structures (Fig. 6). The outward movement of the S4 segment driven by depolarization is coupled to rolling movements of the S1–S3 segments around it and a rolling movement of the entire voltage-sensing module around the pore module (Fig. 6). This movement exerts a torque on the S4–S5 linker, which moves almost parallel to the plane of the intracellular surface of the membrane, induces a bending and twisting motion of the S5 and S6 segments, and opens the pore in an iris-like motion (Fig. 6). These movements are captured in Supplemental Movie S1–3 (Yarov-Yarovoy *et al.* 2011).

Ion selectivity and conductance

The region of the sodium channel that forms the outer end of the pore and the ion selectivity filter was first revealed by identifying the amino acid residues that form the binding site of the pore-blocking toxin tetrodotoxin in the short P loop between S5 and S6 (Noda *et al.* 1989; Terlau *et al.* 1991). Mutations of the same amino acid residues in the pore loop also control ion selectivity (Heinemann *et al.* 1992). This initial view of pore structure of sodium channels has been illuminated at the atomic level by the structure of the Na_VAb channel (Payandeh *et al.* 2011). The activation gate is tightly closed by interactions of the side-chains of Met221 at the intracellular end of the S6 segment in the Na_VAb structure, indicating that this crystal structure has captured the pre-open state, in which all four voltage sensors have activated but the pore has not yet sprung open.

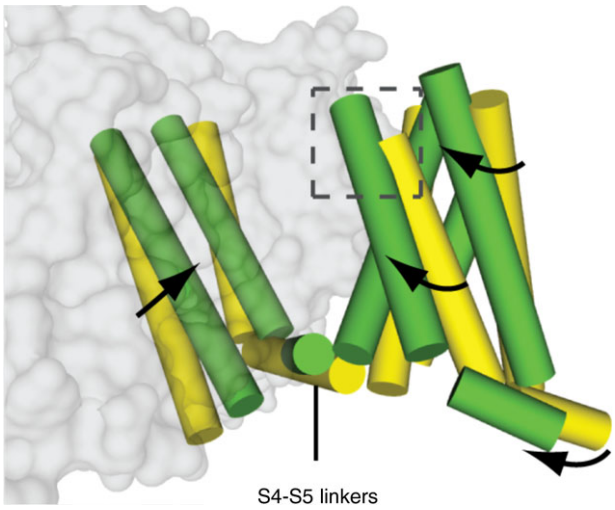

Figure 6. Model for pore opening transition
Superimposition of Na_VAb (yellow; Payandeh *et al.* 2011) and $K_V1.2/2.1$ (green; Long *et al.* 2007) viewed from the membrane.

Although the overall pore architecture of sodium and potassium channels is similar, the structures of their ion selectivity filters and their mechanisms of ion selectivity and conductance are completely different. Potassium channels select K^+ by direct interaction with a series of four ion co-ordination sites formed by the backbone carbonyls of the amino acid residues that comprise the ion selectivity filter (Zhou *et al.* 2001). No water molecules intervene between K^+ and its interacting backbone carbonyls in the ion selectivity filter of potassium channels (Zhou *et al.* 2001). In contrast, the Na_VAb ion selectivity filter has a high-field-strength site at its extracellular end (Fig. 7*A*), formed by the side-chains of four glutamate residues (Payandeh *et al.* 2011), which are highly conserved and are key determinants of ion selectivity in vertebrate sodium and calcium channels (Heinemann *et al.* 1992). Considering its dimensions of $\sim$4.6 Å^2, Na^+ with two planar waters of hydration could fit in this high-field-strength site. This outer site is followed by two ion co-ordination sites formed by backbone carbonyls (Fig. 7*B*). These two carbonyl sites are perfectly designed to bind Na^+ with four planar waters of hydration but would be much too large to bind Na^+ directly. In fact, the Na_VAb selectivity filter is large enough to fit the backbone of the entire potassium channel ion selectivity filter inside it (Payandeh *et al.* 2011). Thus, the chemistry of Na^+ selectivity and conductance is opposite to that of K^+; negatively charged residues interact with Na^+ to remove most (but not all) of its waters of hydration, and Na^+ is conducted as a hydrated ion interacting with the pore through its inner shell of bound water molecules. This structure of the ion selectivity filter of Na_VAb is remarkably similar to the four-barrier, three-site model of ion selectivity, which predicted an outer high-field-strength site that would partly dehydrate the permeating ion and two inner sites that would conduct and rehydrate the permeant Na^+ ion (Hille, 1975*a*). This congruence of theory and structure gives clear insight into the chemistry and biophysics of sodium permeation.

Molecular dynamics simulations of Na_VAb in the pre-open state (Payandeh *et al.* 2011), with the intracellular activation gate closed but the ion selectivity filter in its active state, have yielded additional insight into the permeation process (Fig. 8; Chakrabarti *et al.* 2013). To examine the permeation of Na^+ through the selectivity filter, we performed large-scale molecular dynamics

simulations in an explicit, hydrated lipid bilayer at 0 mV in the presence of 150 mM NaCl, for a total simulation time of 23 μs. Although the cytoplasmic end of the pore is closed, reversible influx and efflux of Na^+ through the selectivity filter occurred spontaneously, leading to equilibrium exchange of Na^+ between the extracellular medium and the central cavity of the channel. The Na^+ bound weakly in the extracellular vestibule, but was strongly co-ordinated at two sites in the selectivity filter, one at Glu177 and one in a box formed by Glu177 carboxyls and Leu176 backbone carbonyls (Fig. 8*A*; Chakrabarti *et al.* 2013). Additional weak binding was detectable to the backbone carbonyls of Thr175 and in the central cavity (Fig. 9*A*; Chakrabarti *et al.* 2013). Analysis of Na^+ dynamics revealed a knock-off mechanism of ion permeation characterized primarily by alternating occupancy of the channel by two and three Na^+ ions, with a computed rate of translocation of $(6 \pm 1) \times 10^6$ ions s^{-1} that is consistent with expectations from electrophysiological studies (Fig. 8*B*; Chakrabarti *et al.* 2013). Although Na^+ ions primarily move in and out of the selectivity filter individually, Na^+ ions also occasionally pass each other in transit and occupy the selectivity filter side by side, in contrast to the strict single filing of K^+ ions in K_V channels. The binding of Na^+ is intimately coupled to the conformational isomerization of the four Glu177 side-chains lining the extracellular end of the selectivity filter. The reciprocal co-ordination of variable numbers of Na^+ ions and carboxylate groups leads to their condensation into ionic clusters of variable charge and spatial arrangement. Structural fluctuations of these ionic clusters result in many accessible ion-binding modes and foster a highly degenerate, liquid-like energy landscape that promotes Na^+ diffusion. By stabilizing multiple ionic occupancy states while helping Na^+ ions diffuse within the selectivity filter, the conformational flexibility of Glu177 side-chains underpins the knock-on mechanism of Na^+ permeation.

A complementary (and contemporaneous) molecular dynamics study of the Na_V channel from *Magnetococcus* sp. (Na_VMs) was based on the open-pore structure derived from X-ray crystallographic studies of the isolated pore domain (Ulmschneider *et al.* 2013). Similarly complex movements of Na^+ and water were observed for unidirectional movement through the open pore as for reversible entry and exit from the pre-open state of Na_VAb, as well as similar occupancy of Na^+ binding sites. High single-channel conductance and high selectivity for Na^+ over K^+ were observed, consistent with well-known functional properties of eukaryotic Na_V channels. The molecular dynamics simulations of these two states of bacterial Na_V channels lay the foundation for detailed mechanistic studies aimed to understand the processes of permeation and selectivity more completely.

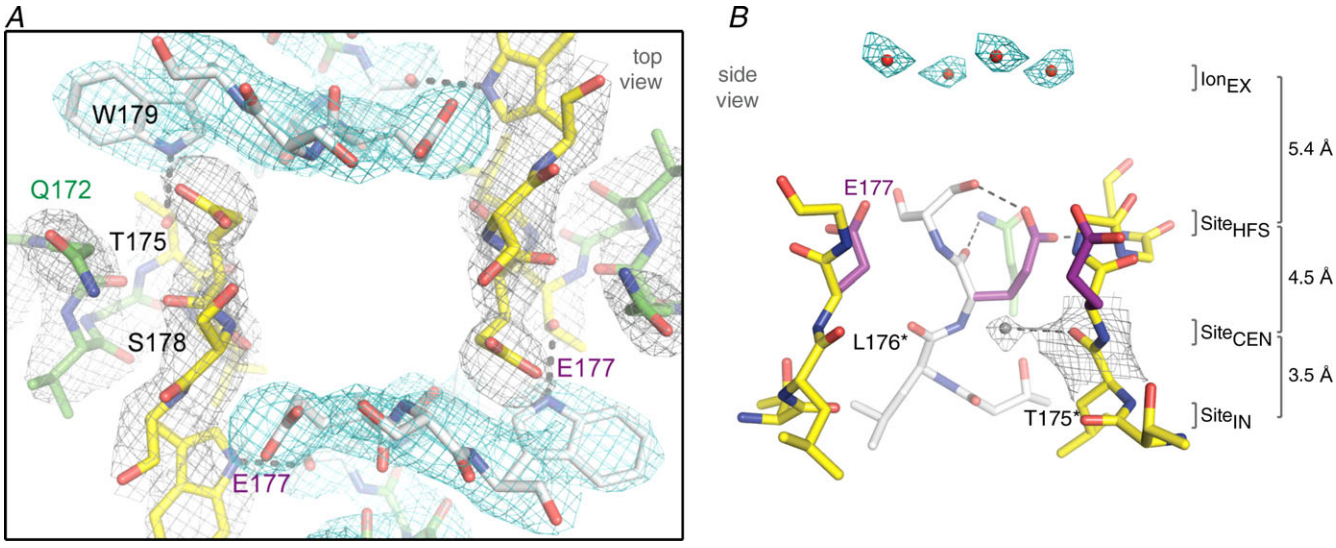

Figure 7. The ion selectivity filter of Na_VAb
A, top view of the ion selectivity filter. Symmetry-related molecules are coloured white and yellow; P helix residues are coloured green. Hydrogen bonds between Thr175 and Trp179 are indicated by grey dashes. Electron densities from F_o–F_c omit maps are contoured at 4.0 σ (blue and grey), and subtle differences can be appreciated (Payandeh *et al.* 2011). *B*, side view of the selectivity filter. Glu177 (purple) interactions with Gln172, Ser178 and the backbone of Ser180 are shown in the far subunit. F_o–F_c omit map, 4.75 σ (blue); putative cations or water molecules (red spheres, Ion$_{EX}$). Electron density around Leu176 (grey; F_o–F_c omit map at 1.75 σ) and a putative water molecule is shown (grey sphere). Na^+ co-ordination sites: Site$_{HFS}$, Site$_{CEN}$ and Site$_{IN}$ (Payandeh *et al.* 2011).

Drug receptor sites in sodium channels

Sodium channels are blocked by drugs used clinically as local anaesthetics, antiarrhythmics and antiepileptics. Site-directed mutagenesis studies of sodium channels revealed the receptor site for local anaesthetics and related drugs, which is formed by amino acid residues in the S6 segments in domains I, III and IV (Fig. 9*A*; Ragsdale *et al.* 1994, 1996; Qu *et al.* 1995; Wang *et al.* 1998; Yarov-Yarovoy *et al.* 2001, 2002). These drugs bind to a common receptor site in the pore of sodium channels and impede ion permeation. The structure of Na_VAb places this drug receptor site in three-dimensional context (Payandeh *et al.* 2011). The amino acid residues that form the receptor sites for sodium channel blockers line the inner surface of the S6 segments and create a three-dimensional drug receptor site whose occupancy would block the pore (Fig. 9*C*). Access to this receptor site by large or hydrophilic drugs would require opening of the intracellular activation gate, which is tightly closed in our structure. This tight closure of the activation gate provides a structural basis for use-dependent block of sodium channels by local anaesthetics and related drugs (Hille, 1977), because they would bind much more rapidly when the channel is opened frequently. Remarkably, consistent with the modulated receptor hypothesis (Hille, 1977), fenestrations lead from the lipid phase of the membrane sideways into the drug receptor site, providing a specific hydrophobic access pathway for drug binding in the resting state of the channel (Fig. 9*C*, pore portals; Payandeh *et al.* 2011). Access to the drug binding site in Na_VAb channels is controlled by the side-chain of a single amino acid residue, Phe203 (Fig. 9*C*; Payandeh *et al.* 2011), which is homologous to amino acid residues identified in previous structure–function studies that control drug access and egress from the local anaesthetic receptor site in mammalian cardiac and brain sodium channels (Ragsdale *et al.* 1994; Qu *et al.* 1995).

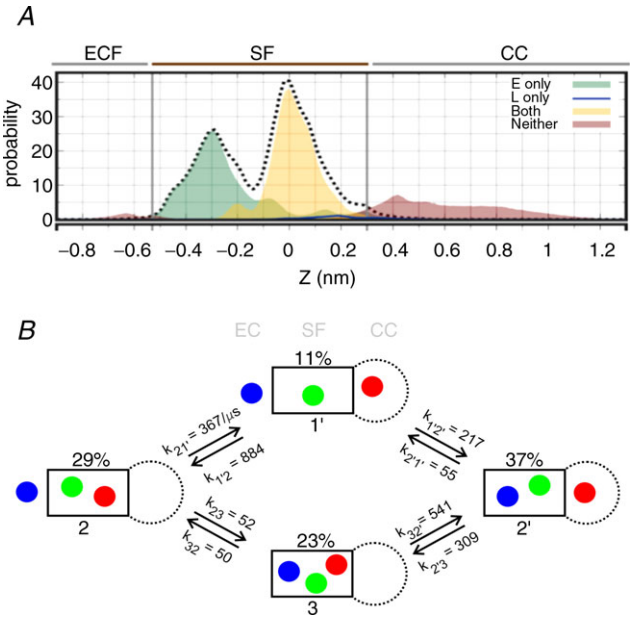

Figure 8. Molecular dynamics of sodium conductance
The entry and exit of sodium ions in the pore of Na_VAb were analysed without constraints for 23 μs at 150 mM Na^+ and $V = 0$. *A*, axial distribution of Na^+ in the selectivity filter (SF) and central cavity (CC), distinguishing between states in which Na^+ is directly bound to Glu177 ('E', green), to both Glu177 and Leu176 ('EL', yellow) or to neither (brown). The selectivity filter is defined by two spatially resolved Na^+ binding sites, E and EL. The small peaks at $z = -0.65$ and $z = 0.40$ nm in the brown distribution correspond to direct Na^+ co-ordination by the hydroxyl O atom of Ser178 and water-mediated co-ordination to the carbonyl O atom of Thr175, respectively. *B*, mechanism and kinetics of Na^+ translocation through the selectivity filter. The black box represents the selectivity filter, with the central cavity to the right and the extracellular mouth to the left. The populations of all four states (**1′**, **2**, **2′** and **3**), which differ in the occupancy of the channel and of the selectivity filter, are shown as percentages, and the rate constants computed from the molecular dynamics trajectories are shown above or below each arrow in units of μs^{-1}. At this ionic concentration (150 mM), states **2** and **2′** correspond to the resting state of the system. The exchange between states **2** and **2′**, which corresponds to a unitary ionic translocation through the selectivity filter, involves either one-ion or three-ion intermediate states (Chakrabarti *et al.* 2013).

Fast inactivation

As first described by Hodgkin & Huxley (1952*c*), sodium channels in eukaryotes open in response to depolarization and then inactivate within 1–2 ms. This fast inactivation process is required for repetitive firing of action potentials in neural circuits and for control of excitability in nerve and muscle cells. Studies with site-directed antipeptide antibodies showed that the short intracellular loop connecting homologous domains III and IV of the sodium channel α subunit is responsible for fast inactivation (Fig. 2; Vassilev *et al.* 1988). This fast inactivation gate serves as an intracellular blocking particle that folds into the channel structure like a hinged lid and blocks the pore during inactivation (Vassilev *et al.* 1988). Binding of a site-directed antibody to this peptide segment results in slowed entry of single channels into the inactivated state (Vassilev *et al.* 1989). Cutting this loop by expression of the sodium channel in two pieces also greatly slows inactivation (Stühmer *et al.* 1989). The key amino acid motif IFM is required to maintain closure of the inactivation gate (West *et al.* 1992), and peptides containing this inactivation gate sequence motif can restore fast inactivation to mutant sodium channels (Eaholtz *et al.* 1994). The inactivation gate bends at a key pair of glycine residues, allowing it to fold into the intracellular mouth of the pore, bind, and block sodium conductance as a hinged lid (Kellenberger *et al.* 1996, 1997*a*,*b*). Analysis of the structure of the inactivation gate by NMR showed that it contains a

rigid α helix preceded by two loops of protein that array the IFM motif and a neighbouring Thr residue on their surface for interaction with and block of the open pore of the channel (Fig. 9*B*, Rohl *et al.* 1999). The fast inactivation gate is not present in homotetrameric bacterial sodium channels, so further structural analysis of the fast inactivation process must await determination of the three-dimensional structure of a eukaryotic sodium channel.

Slow inactivation

Slow inactivation of sodium channels on the time scale of hundreds of milliseconds to seconds was also first observed in the squid giant axon (Adelman & Palti, 1969; Rudy, 1978). The molecular mechanism of slow inactivation is less well defined than fast inactivation, but extensive structure–function studies implicate conformational changes in the selectivity filter (Balser *et al.* 1996; Todt *et al.* 1999; Vilin *et al.* 2001; Hilber *et al.* 2005; Pavlov *et al.* 2005) and the S6 segment (Zhao *et al.* 2004*a*,*b*; Chen *et al.* 2006) as key steps in the transition to the slow-inactivated state. The initial crystallographic studies of the Na_VAb bacterial sodium channel focused on the I217C mutant, because this mutation substantially increased the resolution of the structure determination of the pre-open state (Payandeh *et al.* 2011). The wild-type Na_VAb channel has very prominent use-dependent slow inactivation (Fig. 10*A*). An early phase of slow inactivation occurs during test pulses, and the composite time constant for this phase of slow inactivation approaches 20 ms at positive membrane potentials (Fig. 10*A*). In addition, repetitive depolarizations at slow rates (0.2 or 1 Hz; Fig. 10*A*) elict a late phase of slow inactivation that reduces the sodium current to near zero and is very slowly reversible. Solubilization and purification would be

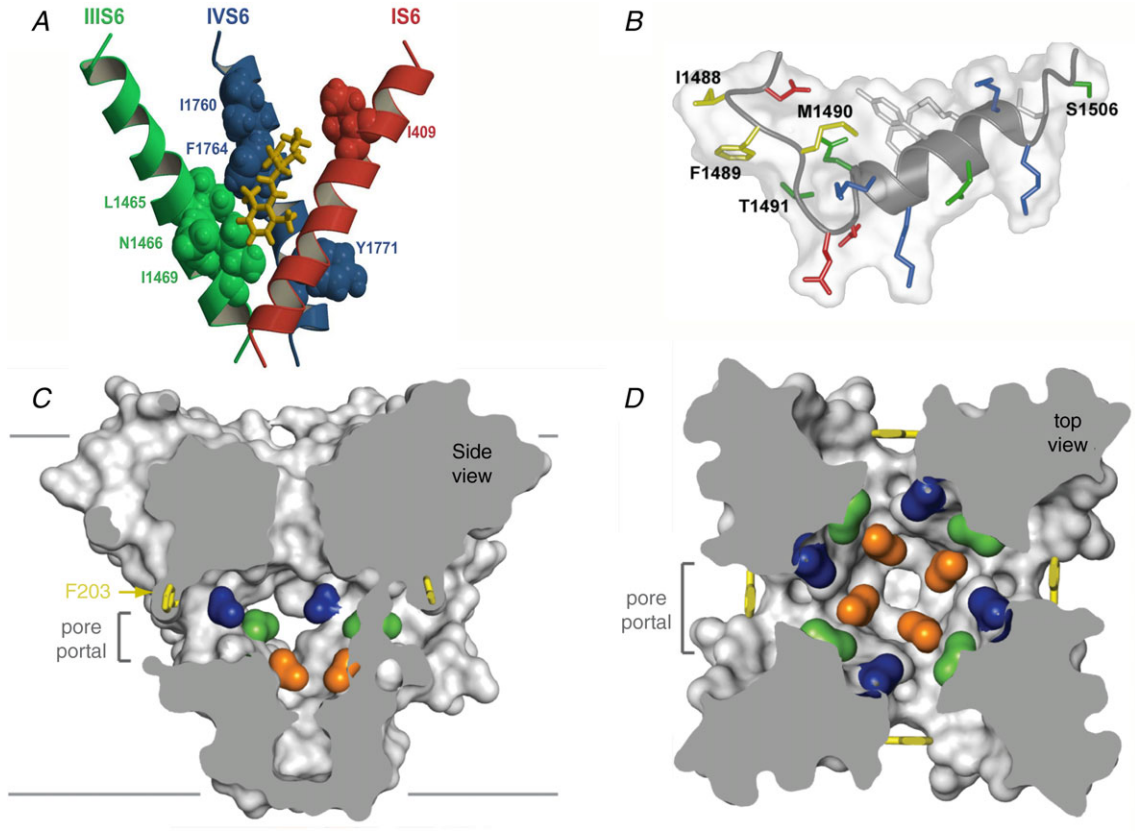

Figure 9. Drug receptor site and fast inactivation gate
A, model of the local anaesthetic receptor site in mammalian $Na_V1.2$ channels (Yarov-Yarovoy *et al.* 2002). *B*, structure of the inactivation gate of mammalian $Na_V1.2$ channels in solution determined by NMR (Rohl *et al.* 1999). *C*, side view through the pore module, illustrating fenestrations (portals) and hydrophobic access to central cavity. Phe203 side-chains are shown as yellow sticks. Surface representations of Na_VAb residues aligning with those implicated in drug binding and block are shown as follows: blue, Thr206; green, Met209; and orange, Val213. Membrane boundaries are shown as grey lines. Electron density from an F_o–F_c omit map is contoured at 2.0 σ. *D*, top view sectioned below the selectivity filter, coloured as in *C* (Payandeh *et al.* 2011).

expected to drive Na_VAb into this very stable inactivated state, and wild-type Na_VAb crystallizes in a different conformation that has the structure expected of the slow-inactivated state (Payandeh *et al.* 2012). The selectivity filter, central cavity and intracellular activation gate have all been modified by an asymmetric pore collapse, in which two of the S6 segments move toward the central axis of the pore and two move away to give a striking dimer-of-dimers arrangement (Fig. 10*B*; Payandeh *et al.* 2012). A similar conformation is observed in the crystal structure of the distantly related bacterial sodium channel Na_VRh (Zhang *et al.* 2012). It is likely that this pore collapse is responsible for the stability of the slow-inactivated state and the long time required for recovery from slow inactivation.

Conclusion

The structure of the slow inactivated state completes our tour through the functional states of sodium channels, including voltage sensing and activation, pore opening, sodium selectivity and conductance, drug block, and fast and slow inactivation. Discovery of the sodium channel protein, studies of its structure and function by a combination of molecular biology and electrophysiology, and analysis of its structure in multiple states by x-ray crystallography and high-resolution protein modelling have given us a clear set of molecular models for each step in this functional cycle of sodium channels. To illustrate these advances, the Supplemental Movie (Supplemental Movie S4) integrates structural information from studies of bacterial and mammalian sodium channels to produce a

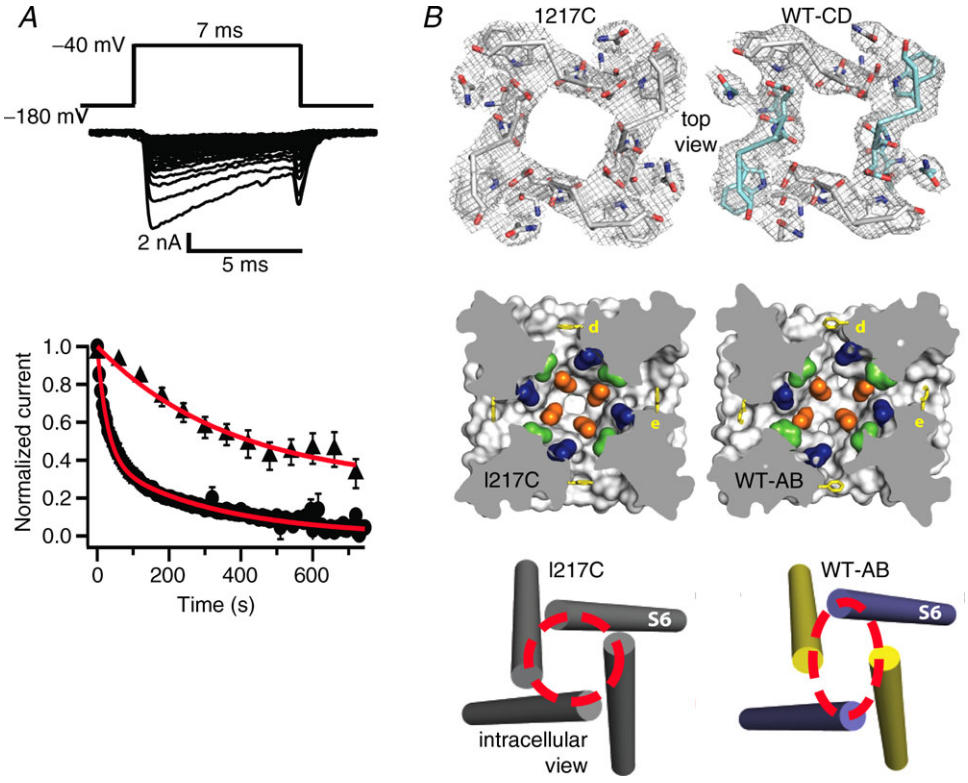

Figure 10. Structure of the slow-inactivated state in Na_VAb
A, use-dependent development of slow inactivation. Depolarizations from a holding potential of −180 mV to −40 mV, 7 ms in duration, were applied at 0.2 Hz (filled circles) or once per minute (filled triangles), and the peak current elicited by each pulse was measured. Currents were normalized to the peak inward current during the first pulse. *B*, top diagrams shown the selectivity filter as stick representations with a $2F_o–F_c$ map calculated at 3.2 Å resolution (grey mesh) contoured at 1.5 σ for Na_VAb -I217C and 1.0 σ for Na_VAb -CD. Symmetry-related subunits in WT-CD are coloured white (chains A and D) and cyan (chains B and C), respectively. Middle diagrams illustrate the central cavity. A view through the pore module sectioned below the selectivity filter illustrates the lateral pore fenestrations, hydrophobic access to the central cavity, and structural asymmetry in the Na_VAb-AB pore domain. Phe203 side-chains are yellow sticks. Na_VAb residues implicated in drug binding in vertebrate Na_V channels are coloured as follows: blue, Thr206; green, Met209; and orange, Val213. Bottom diagrams illustrate the activation gate. Red dashed lines indicate the C_α location of D219 (the last S6 residue modelled in WT-AB), where the S6 helices are shown as cylinders. Colurs are as follows: purple, WT chain A; and yellow, WTchain B (Payandeh *et al.* 2012).

complete working model of a mammalian sodium channel with a complete pore domain, a single voltage sensor (for clarity) and an inactivation gate (Supplemental Movie S4). Running the Movie shows the outward movement of the S4 gating charges, the exchange of ion-pair partners that takes place as they move, the rolling motion of the S1–S3 segments around the S4 segment, the consequent rolling motion of the voltage sensor around the lateral surface of the pore domain, the torque on the S4–S5 segment as it move along the plane of the inner membrane surface to pull on the S5 and S6 segments, the subtle bending and twisting motion of the S6 segments and the opening of the pore. As the pore opens, sodium ions enter from outside the cell, and the fast inactivation gate closes to terminate sodium conductance Amazingly, this series of conformational transitions takes place within 2 ms and generates the electrical signals that are responsible for information encoding and transmission in the brain, action potential conduction in nerves, contraction of muscles and many other physiological processes. Looking ahead, one can anticipate more detailed views of these structural and functional transitions from X-ray crystal structures of the sodium channel in resting, open and fast-inactivated states. New crystal structures and structure–function studies will also reveal the domain-specific specializations in the four-domain eukaryotic Na_V channels, which have already been well described at the functional level for the pore module (Heinemann *et al.* 1992; Favre *et al.* 1996) and the voltage sensors (Chanda & Bezanilla, 2002; Capes *et al.* 2013). Moreover, the detailed structure of the drug receptor site(s) on sodium channel will provide the foundation for structure-based design of new generations of subtype-specific sodium channel therapeutics for treatment of epilepsy, chronic pain and cardiac arrhythmia, with greater efficacy and fewer unwanted side-effects.

Call for comments

Readers are invited to give their opinion on this article. To submit a comment, go to: http://ep.physoc.org/letters/submit/expphysiol;99/1/35.

References

Adelman WJ Jr & Palti Y (1969). The effects of external potassium and long duration voltage conditioning on the amplitude of sodium currents in the giant axon of the squid, *Loligo pealei*. *J Gen Physiol* **54**, 589–606.

Armstrong CM (1971). Interaction of tetraethylammonium ion derivatives with the potassium channels of giant axon. *J Gen Physiol* **58**, 413–437.

Armstrong CM (1981). Sodium channels and gating currents. *Physiol Rev* **61**, 644–682.

Armstrong CM & Bezanilla F (1973). Currents related to movement of the gating particles of the sodium channels. *Nature* **242**, 459–461.

Armstrong CM & Benzanilla F (1974). Charge movement associated with the opening and closing of the activation gates of the Na channels. *J Gen Physiol* **63**, 533–552.

Armstrong CM & Bezanilla F (1977). Inactivation of the sodium channel. II. Gating current experiments. *J Gen Physiol* **70**, 567–590.

Armstrong CM, Bezanilla F & Rojas E (1973). Destruction of sodium conductance inactivation in squid axons perfused with pronase. *J Gen Physiol* **62**, 375–391.

Balser JR, Nuss HB, Chiamvimonvat N, Pérez-García MT, Marban E & Tomaselli GF (1996). External pore residue mediates slow inactivation in μ1 rat skeletal muscle sodium channels. *J Physiol* **494**, 431–442.

Beneski DA & Catterall WA (1980). Covalent labeling of protein components of the sodium channel with a photoactivable derivative of scorpion toxin. *Proc Natl Acad Sci U S A* **77**, 639–643.

Bezanilla F & Armstrong CM (1977). Inactivation of the sodium channel. I. Sodium current experiments. *J Gen Physiol* **70**, 549–566.

Brackenbury WJ & Isom LL (2011). Na channel β subunits: overachievers of the ion channel family. *Front Pharmacol* **2**, 53.

Broomand A & Elinder F (2008). Large-scale movement within the voltage-sensor paddle of a potassium channel–support for a helical-screw motion. *Neuron* **59**, 770–777.

Campos FV, Chanda B, Roux B & Bezanilla F (2007). Two atomic constraints unambiguously position the S4 segment relative to S1 and S2 segments in the closed state of Shaker K channel. *Proc Natl Acad Sci U S A* **104**, 7904–7909.

Capes DL, Goldschen-Ohm MP, Arcisio-Miranda M, Bezanilla F & Chanda B (2013). Domain IV voltage-sensor movement is both sufficient and rate limiting for fast inactivation in sodium channels. *J Gen Physiol* **142**, 101–112.

Catterall WA (1979). Binding of scorpion toxin to receptor sites associated with sodium channels in frog muscle. Correlation of voltage-dependent binding with activation. *J Gen Physiol* **74**, 375–391.

Catterall WA (1980). Neurotoxins that act on voltage-sensitive sodium channels in excitable membranes. *Annu Rev Pharmacol Toxicol* **20**, 15–43.

Catterall WA (1986*a*). Molecular properties of voltage-sensitive sodium channels. *Annu Rev Biochem* **55**, 953–985.

Catterall WA (1986*b*). Voltage-dependent gating of sodium channels: correlating structure and function. *Trends Neurosci* **9**, 7–10.

Catterall WA (2000). From ionic currents to molecular mechanisms: the structure and function of voltage-gated sodium channels. *Neuron* **26**, 13–25.

Catterall WA (2010). Ion channel voltage sensors: structure, function, and pathophysiology. *Neuron* **67**, 915–928.

Catterall WA, Cestèle S, Yarov-Yarovoy V, Yu FH, Konoki K & Scheuer T (2007). Voltage-gated ion channels and gating modifier toxins. *Toxicon* **49**, 124–141.

Cestèle S, Qu Y, Rogers JC, Rochat H, Scheuer T & Catterall WA (1998). Voltage sensor-trapping: enhanced activation of sodium channels by β-scorpion toxin bound to the S3–S4 loop in domain II. *Neuron* **21**, 919–931.

Cestèle S, Yarov-Yarovoy V, Qu Y, Sampieri F, Scheuer T & Catterall WA (2006). Structure and function of the voltage sensor of sodium channels probed by a β-scorpion toxin. *J Biol Chem* **281**, 21332–21344.

Chakrabarti N, Ing C, Payandeh J, Zheng N, Catterall WA & Pomes R (2013). Catalysis of Na^+ permeation in the bacterial sodium channel Na_VAb. *Proc Natl Acad Sci U S A* **110**, 11331–11336.

Chanda B, Asamoah OK, Blunck R, Roux B & Bezanilla F (2005). Gating charge displacement in voltage-gated ion channels involves limited transmembrane movement. *Nature* **436**, 852–856.

Chanda B & Bezanilla F (2002). Tracking voltage-dependent conformational changes in skeletal muscle sodium channel during activation. *J Gen Physiol* **120**, 629–645.

Chen Y, Yu FH, Surmeier DJ, Scheuer T & Catterall WA (2006). Neuromodulation of Na^+ channel slow inactivation via cAMP-dependent protein kinase and protein kinase C. *Neuron* **49**, 409–420.

DeCaen PG, Yarov-Yarovoy V, Scheuer T & Catterall WA (2011). Gating charge interactions with the S1 segment during activation of a Na^+ channel voltage sensor. *Proc Natl Acad Sci U S A* **108**, 18825–18830.

DeCaen PG, Yarov-Yarovoy V, Sharp EM, Scheuer T & Catterall WA (2009). Sequential formation of ion pairs during activation of a sodium channel voltage sensor. *Proc Natl Acad Sci U S A* **106**, 22498–22503.

DeCaen PG, Yarov-Yarovoy V, Zhao Y, Scheuer T & Catterall WA (2008). Disulfide locking a sodium channel voltage sensor reveals ion pair formation during activation. *Proc Natl Acad Sci U S A* **105**, 15142–15147.

DeCaen PG (2010). The mechanism of voltage dependent gating of he NaChBac prokaryotic sodium channel. Unpublished doctoral dissertation. University of Washington, Seattle, WA.

Eaholtz G, Scheuer T & Catterall WA (1994). Restoration of inactivation and block of open sodium channels by an inactivation gate peptide. *Neuron* **12**, 1041–1048.

Favre I, Moczydlowski E & Schild L (1996). On the structural basis for ionic selectivity among Na^+, K^+, and Ca^{2+} in the voltage-gated sodium channel. *Biophys J* **71**, 3110–3125.

Goldin AL, Snutch T, Lubbert H, Dowsett A, Marshall J, Auld V, Downey W, Fritz LC, Lester HA, Dunn R, Catterall WA & Davidson N (1986). Messenger RNA coding for only the α subunit of the rat brain Na channel is sufficient for expression of functional channels in *Xenopus* oocytes. *Proc Natl Acad Sci U S A* **83**, 7503–7507.

Guy HR & Seetharamulu P (1986). Molecular model of the action potential sodium channel. *Proc Natl Acad Sci U S A* **508**, 508–512.

Hartshorne RP & Catterall WA (1981). Purification of the saxitoxin receptor of the sodium channel from rat brain. *Proc Natl Acad Sci U S A* **78**, 4620–4624.

Hartshorne RP & Catterall WA (1984). The sodium channel from rat brain. Purification and subunit composition. *J Biol Chem* **259**, 1667–1675.

Hartshorne RP, Keller BU, Talvenheimo JA, Catterall WA & Montal M (1985). Functional reconstitution of the purified brain sodium channel in planar lipid bilayers. *Proc Natl Acad Sci U S A* **82**, 240–244.

Hartshorne RP, Messner DJ, Coppersmith JC & Catterall WA (1982). The saxitoxin receptor of the sodium channel from rat brain. Evidence for two nonidentical β subunits. *J Biol Chem* **257**, 13888–13891.

Heinemann SH, Terlau H, Stühmer W, Imoto K & Numa S (1992). Calcium channel characteristics conferred on the sodium channel by single mutations. *Nature* **356**, 441–443.

Hilber K, Sandtner W, Zarrabi T, Zebedin E, Kudlacek O, Fozzard HA & Todt H (2005). Selectivity filter residues contribute unequally to pore stabilization in voltage-gated sodium channels. *Biochemistry* **44**, 13874–13882.

Hille B (1971). The permeability of the sodium channel to organic cations in myelinated nerve. *J Gen Physiol* **59**, 599–619.

Hille B (1972). The permeability of the sodium channel to metal cations in myelinated nerve. *J Gen Physiol* **59**, 637–658.

Hille B (1975*a*). Ionic selectivity, saturation, and block in sodium channels. A four-barrier model. *J Gen Physiol* **66**, 535–560.

Hille B (1975*b*). The receptor for tetrodotoxin and saxitoxin: a structural hypothesis. *Biophys J* **15**, 615–619.

Hille B (1977). Local anesthetics: hydrophilic and hydrophobic pathways for the drug-receptor reaction. *J Gen Physiol* **69**, 497–515.

Hille B (2001). *Ionic Channels of Excitable Membranes*, 3rd edition. Sinauer Associates Inc., Sunderland, MA, USA.

Hodgkin AL & Huxley AF (1952*a*). Currents carried by sodium and potassium ions through the membrane of the giant axon of *Loligo*. *J Physiol* **116**, 449–472.

Hodgkin AL & Huxley AF (1952*b*). The components of membrane conductance in the giant axon of *Loligo*. *J Physiol* **116**, 473–496.

Hodgkin AL & Huxley AF (1952*c*). The dual effect of membrane potential on sodium conductance in the giant axon of *Loligo*. *J Physiol* **116**, 497–506.

Hodgkin AL & Huxley AF (1952*d*). A quantitative description of membrane current and its application to conduction and excitation in nerve. *J Physiol* **117**, 500–544.

Isom LL, De Jongh KS, Patton DE, Reber BFX, Offord J, Charbonneau H, Walsh K, Goldin AL & Catterall WA (1992). Primary structure and functional expression of the β1 subunit of the rat brain sodium channel. *Science* **256**, 839–842.

Isom LL, Ragsdale DS, De Jongh KS, Westenbroek RE, Reber BFX, Scheuer T & Catterall WA (1995). Structure and function of the β2 subunit of brain sodium channels, a transmembrane glycoprotein with a CAM-motif. *Cell* **83**, 433–442.

Kazarinova-Noyes K, Malhotra JD, McEwen DP, Mattei LN, Berglund EO, Ranscht B, Levinson SR, Schachner M, Shrager P, Isom LL & Xiao ZC (2001). Contactin associates with sodium channels and increases their functional expression. *J Neurosci* **21**, 7517–7525.

Kellenberger S, Scheuer T & Catterall WA (1996). Movement of the Na^+ channel inactivation gate during inactivation. *J Biol Chem* **271**, 30971–30979.

Kellenberger S, West JW, Catterall WA & Scheuer T (1997*a*). Molecular analysis of potential hinge residues in the inactivation gate of brain type IIA Na^+ channels. *J Gen Physiol* **19**, 607–617.

Kellenberger S, West JW, Scheuer T & Catterall WA (1997*b*). Molecular analysis of the putative inactivation particle in the inactivation gate of brain type IIA Na^+ channels. *J Gen Physiol* **109**, 589–605.

Keynes RD & Rojas E (1974). Kinetics and steady-state properties of the charged system controlling sodium conductance in the squid giant axon. *J Physiol* **239**, 393–434.

Koishi R, Xu H, Ren D, Navarro B, Spiller BW, Shi Q & Clapham DE (2004). A superfamily of voltage-gated sodium channels in bacteria. *J Biol Chem* **279**, 9532–9538.

Kontis KJ, Rounaghi A & Goldin AL (1997). Sodium channel activation gating is affected by substitutions of voltage sensor positive charges in all four domains. *J Gen Physiol* **110**, 391–401.

Lin MC, Hsieh JY, Mock AF & Papazian DM (2011). R1 in the Shaker S4 occupies the gating charge transfer center in the resting state. *J Gen Physiol* **138**, 155–163.

Long SB, Campbell EB & Mackinnon R (2005*a*). Crystal structure of a mammalian voltage-dependent *Shaker* family K^+ channel. *Science* **309**, 897–903.

Long SB, Campbell EB & Mackinnon R (2005*b*). Voltage sensor of Kv1.2: structural basis of electromechanical coupling. *Science* **309**, 903–908.

Long SB, Tao X, Campbell EB & MacKinnon R (2007). Atomic structure of a voltage-dependent K^+ channel in a lipid membrane-like environment. *Nature* **450**, 376–382.

Malhotra JD, Kazen-Gillespie K, Hortsch M & Isom LL (2000). Sodium channel β subunits mediate homophilic cell adhesion and recruit ankyrin to points of cell-cell contact. *J Biol Chem* **275**, 11383–11388.

Noda M, Ikeda T, Suzuki T, Takeshima H, Takahashi T, Kuno M & Numa S (1986). Expression of functional sodium channels from cloned cDNA. *Nature* **322**, 826–828.

Noda M, Shimizu S, Tanabe T, Takai T, Kayano T, Ikeda T, Takahashi H, Nakayama H, Kanaoka Y, Minamino N, Kangawa K, Matsuo H, Raftery M, Hirose T, Inayama S, Hayashida H, Miyata T & Numa S (1984). Primary structure of Electrophorus electricus sodium channel deduced from cDNA sequence. *Nature* **312**, 121–127.

Noda M, Suzuki H, Numa S & Stühmer W (1989). A single point mutation confers tetrodotoxin and saxitoxin insensitivity on the sodium channel II. *FEBS Lett* **259**, 213–216.

Pavlov E, Bladen C, Winkfein R, Diao C, Dhaliwal P & French RJ (2005). The pore, not cytoplasmic domains, underlies inactivation in a prokaryotic sodium channel. *Biophys J* **89**, 232–242.

Payandeh J, Gamal El-Din TM, Scheuer T, Zheng N & Catterall WA (2012). Crystal structure of a voltage-gated sodium channel in two potentially inactivated states. *Nature* **486**, 135–139.

Payandeh J, Scheuer T, Zheng N & Catterall WA (2011). The crystal structure of a voltage-gated sodium channel. *Nature* **475**, 353–358.

Qu Y, Rogers J, Tanada T, Scheuer T & Catterall WA (1995). Molecular determinants of drug access to the receptor site for antiarrhythmic drugs in the cardiac Na^+ channel. *Proc Natl Acad Sci U S A* **270**, 25696–25701.

Ragsdale DS, McPhee JC, Scheuer T & Catterall WA (1994). Molecular determinants of state-dependent block of sodium channels by local anesthetics. *Science* **265**, 1724–1728.

Ragsdale DR, McPhee JC, Scheuer T & Catterall WA (1996). Common molecular determinants of local anesthetic, antiarrhythmic, and anticonvulsant block of voltage-gated Na^+ channels. *Proc Natl Acad Sci U S A* **93**, 9270–9275.

Ratcliffe CF, Qu Y, McCormick KA, Tibbs VC, Dixon JE, Scheuer T & Catterall WA (2000). A sodium channel signaling complex: modulation by associated receptor protein tyrosine phosphatase β. *Nat Neurosci* **3**, 437–444.

Ratcliffe CF, Westenbroek RE, Curtis R & Catterall WA (2001). Sodium channel β1 and β3 subunits associate with neurofascin through their extracellular immunoglobulin-like domain. *J Cell Biol* **154**, 427–434.

Ren D, Navarro B, Xu H, Yue L, Shi Q & Clapham DE (2001). A prokaryotic voltage-gated sodium channel. *Science* **294**, 2372–2375.

Rogers JC, Qu Y, Tanada TN, Scheuer T & Catterall WA (1996). Molecular determinants of high affinity binding of α-scorpion toxin and sea anemone toxin in the S3–S4 extracellular loop in domain IV of the Na^+ channel α subunit. *J Biol Chem* **271**, 15950–15962.

Rohl CA, Boeckman FA, Baker C, Scheuer T, Catterall WA & Klevit RE (1999). Solution structure of the sodium channel inactivation gate. *Biochemistry* **38**, 855–861.

Rudy B (1978). Slow inactivation of the sodium conductance in squid giant axons. Pronase resistance. *J Physiol* **283**, 1–21.

Shafrir Y, Durell SR & Guy HR (2008). Models of voltage-dependent conformational changes in NaChBac channels. *Biophys J* **95**, 3663–3676.

Srinivasan J, Schachner M & Catterall WA (1998). Interaction of voltage-gated sodium channels with the extracellular matrix molecules tenascin-C and tenascin-R. *Proc Natl Acad Sci U S A* **95**, 15753–15757.

Starace DM & Bezanilla F (2004). A proton pore in a potassium channel voltage sensor reveals a focused electric field. *Nature* **427**, 548–553.

Stühmer W, Conti F, Suzuki H, Wang X, Noda M, Yahadi N, Kubo H & Numa S (1989). Structural parts involved in activation and inactivation of the sodium channel. *Nature* **339**, 597–603.

Talvenheimo JA, Tamkun MM & Catterall WA (1982). Reconstitution of neurotoxin-stimulated sodium transport by the voltage-sensitive sodium channel purified from rat brain. *J Biol Chem* **257**, 11868–11871.

Tamkun MM, Talvenheimo JA & Catterall WA (1984). The sodium channel from rat brain. Reconstitution of neurotoxin-activated ion flux and scorpion toxin binding from purified components. *J Biol Chem* **259**, 1676–1688.

Tao X, Lee A, Limapichat W, Dougherty DA & MacKinnon R (2010). A gating charge transfer center in voltage sensors. *Science* **328**, 67–73.

Terlau H, Heinemann SH, Stühmer W, Pusch M, Conti F, Imoto K & Numa S (1991). Mapping the site of block by tetrodotoxin and saxitoxin of sodium channel II. *FEBS Lett* **293**, 93–96.

Todt H, Dudley SC, Kyle JW, French RJ & Fozzard HA (1999). Ultra-slow inactivation in μ1 Na^+ channels is produced by a structural rearrangement of the outer vestibule. *Biophys J* **76**, 1335–1345.

Ulmschneider MB, Bagnéris C, McCusker EC, DeCaen PG, Delling M, Clapham DE, Ulmschneider JP & Wallace BA (2013). Molecular dynamics of ion transport through the open conformation of a bacterial voltage-gated sodium channel. *Proc Natl Acad Sci U S A* **110**, 6364–6369.

Vargas E, Yarov-Yarovoy V, Khalili-Araghi F, Catterall WA, Klein ML, Tarek M, Lindahl E, Schulten K, Perozo E, Bezanilla F & Roux B (2012). An emerging consensus on voltage-dependent gating from computational modeling and molecular dynamics simulations. *J Gen Physiol* **140**, 587–594.

Vassilev PM, Scheuer T & Catterall WA (1988). Identification of an intracellular peptide segment involved in sodium channel inactivation. *Science* **241**, 1658–1661.

Vassilev P, Scheuer T & Catterall WA (1989). Inhibition of inactivation of single sodium channels by a site-directed antibody. *Proc Natl Acad Sci U S A* **86**, 8147–8151.

Vilin YY, Fujimoto E & Ruben PC (2001). A single residue differentiates between human cardiac and skeletal muscle Na^+ channel slow inactivation. *Biophys J* **80**, 2221–2230.

Wang GK, Quan C & Wang S (1998). A common local anesthetic receptor for benzocaine and etidocaine in voltage-gated mu1 Na^+ channels. *Pflugers Arch* **435**, 293–302.

Wang J, Yarov-Yarovoy V, Kahn R, Gordon D, Gurevitz M, Scheuer T & Catterall WA (2011). Mapping the receptor site for α-scorpion toxins on a Na^+ channel voltage sensor. *Proc Natl Acad Sci U S A* **108**, 15426–15431.

West JW, Patton DE, Scheuer T, Wang Y, Goldin AL & Catterall WA (1992). A cluster of hydrophobic amino acid residues required for fast Na^+ channel inactivation. *Proc Natl Acad Sci U S A* **89**, 10910–10914.

Yang N, George AL Jr & Horn R (1996). Molecular basis of charge movement in voltage-gated sodium channels. *Neuron* **16**, 113–122.

Yang N & Horn R (1995). Evidence for voltage-dependent S4 movement in sodium channel. *Neuron* **15**, 213–218.

Yarov-Yarovoy V, Baker D & Catterall WA (2006). Voltage sensor conformations in the open and closed states in ROSETTA structural models of K^+ channels. *Proc Natl Acad Sci U S A* **103**, 7292–7297.

Yarov-Yarovoy V, Brown J, Sharp E, Clare JJ, Scheuer T & Catterall WA (2001). Molecular determinants of voltage-dependent gating and binding of pore-blocking drugs in transmembrane segment IIIS6 of the Na^+ channel α subunit. *J Biol Chem* **276**, 20–27.

Yarov-Yarovoy V, DeCaen PG, Westenbroek RE, Pan CY, Scheuer T, Baker D & Catterall WA (2011). Structural basis for gating charge movement in the voltage sensor of a sodium channel. *Proc Natl Acad Sci U S A* **109**, E93–E102.

Yarov-Yarovoy V, McPhee JC, Idsvoog D, Pate C, Scheuer T & Catterall WA (2002). Role of amino acid residues in transmembrane segments IS6 and IIS6 of the sodium channel α subunit in voltage-dependent gating and drug block. *J Biol Chem* **277**, 35393–35401.

Yu FH & Catterall WA (2004). The VGL-chanome: a protein superfamily specialized for electrical signaling and ionic homeostasis. *Sci STKE* **2004**, re15.

Zhang JZ, Yarov-Yarovoy V, Scheuer T, Karbat I, Cohen L, Gordon D, Gurevitz M & Catterall WA (2011). Structure-function map of the receptor site for β-scorpion toxins in domain II of voltage-gated sodium channels. *J Biol Chem* **286**, 33641–33651.

Zhang X, Ren W, DeCaen P, Yan C, Tao X, Tang L, Wang J, Hasegawa K, Kumasaka T, He J, Wang J, Clapham DE & Yan NY (2012). Crystal structure of an orthologue of the NaChBac voltage-gated sodium channel. *Nature* **486**, 130–134.

Zhao Y, Scheuer T & Catterall WA (2004*a*). Reversed voltage-dependent gating of a bacterial sodium channel with proline substitutions in the S6 transmembrane segment. *Proc Natl Acad Sci U S A* **101**, 17873–17878.

Zhao Y, Yarov-Yarovoy V, Scheuer T & Catterall WA (2004*b*). A gating hinge in Na^+ channels; a molecular switch for electrical signaling. *Neuron* **41**, 859–865.

Zhou Y, Morais-Cabral JH, Kaufman A & MacKinnon R (2001). Chemistry of ion coordination and hydration revealed by a potassium channel–Fab complex at 2.0 Å resolution. *Nature* **414**, 43–48.

Additional Information

Competing interests

None declared.

Funding

Research reported in this publication was supported by the National Institute of Neurological Disorders and Stroke (NINDS) of the National Institutes of Health under award number R01NS015751. The content is solely the responsibility of the authors and does not necessarily represent the official views of the National Institutes of Health.

Acknowledgements

I would like to thank my collaborators Todd Scheuer and Ning Zheng (Department of Pharmacology, University of Washington), Rachel Klevit and David Baker (Department of Biochemistry, University of Washington), and Régis Pomès (Hospital for Sick Children and University of Toronto), whose work is illustrated in the figures presented here.

Supplementary Information

The following supporting information is available in the online version of this article.

Movie S1. Side view of NaChBac channel. A single voltage-sensing module is depicted, linked to a complete pore

module. Movie illustrates movement of voltage sensor and pore during activation and pore opening by connecting several states demonstrated by disulfide locking, molecular modeling with Rosetta, and x-ray crystallography.

Movie S2. Extracellular view of NaChBac. A single voltage-sensing module is depicted, linked to a complete pore module. Movie illustrates movement of voltage sensor and pore during activation and pore opening by connecting several states demonstrated by disulfide locking, molecular modeling with Rosetta, and x-ray crystallography.

Movie S3. Intracellular view of NaChBac. A single voltage-sensing module is depicted, linked to a complete pore module. Movie illustrates movement of voltage sensor and pore during activation and pore opening by connecting several states demonstrated by disulfide locking, molecular modeling with Rosetta, and x-ray crystallography.

Movie S4. Side view of a model of the mammalian NaV channel with an inactivation gate. Drawn from Movie 1 with attachment with the structure of the inactivation gate from a mammalian NaV channel added (see text).